IFSCC 35TH CONGRESS
FRANCE_CANNES 15-18 SEPT 25
THE FUTURE IS SCIENCE
ifscc2025.com

Holotomographic Microscopy for Pigmentation Control"

Mengjing Bao[1], Jörg Kremp[1] and Remo Campiche[1,*]

[1] dsm-firmenich, Kaiseraugst, Switzerland

1. Introduction

Melanogenesis is a complex biochemical process that occurs within specialized organelles called melanosomes in melanocytes. The process begins with the amino acid L-Tyrosine, which is oxidized to dopaquinone by the enzyme tyrosinase (TYR). This rate-limiting step initiates a series of reactions that lead to the production of two types of melanin: eumelanin (brown-black pigment) and pheomelanin (yellow-red pigment) [1]. Once synthesized, melanin is packaged into melanosomes within the perinuclear region of melanocytes [2]. Melanosome formation and maturation are highly regulated processes essential for melanin synthesis and intracellular transport. Melanosomes progress through four distinct stages of development. Stage I melanosomes are early endosomal-like structures lacking pigment. In Stage II, they acquire a fibrillar matrix, providing a scaffold for melanin deposition. Stage III melanosomes begin melanin synthesis, gradually accumulating pigment. Finally, Stage IV melanosomes are fully melanized, functioning as mature organelles ready for transport and transfer to keratinocytes [2, 3]

Traditionally, *in vitro* efficacy testing of bioactive compounds has primarily focused on directly measuring melanin content, as well as assessing gene expression and enzyme activity involved in melanin biosynthesis and transfer [4]. These methods fail to capture melanosome dynamic within cells, limiting their ability to fully assess the effects of bioactive compounds.

We propose a novel imaging-based screening assay using holotomography microscopy (HTM) to overcome these limitations by enabling real-time visualization and quantitative analysis of melanosome dynamics [5]. HTM is a cutting-edge imaging technique that integrates holography and tomography principles to enable high-resolution, three-dimensional imaging of biological specimens without the need for labels. HTM works on the principle of quantitative phase imaging. It uses holography to capture the interference pattern between light that has passed through a sample and a reference beam. These interference patterns contain information about both the amplitude and phase of the transmitted light, which are related to the refractive index (RI) of the sample. These holograms are then computationally reconstructed to create a 3D RI tomogram of the sample [6].

The melanosomes (Stage III and Stage IV), which are filled with melanin, have a distinct RI compared to the surrounding cytoplasm or other cellular structures [7, 8]. HTM can detect these differences in RI, allowing the melanosomes to be visualized without the need for staining. The ability of HTM to measure phase shifts quantitatively allows researchers to analyze the size, shape, number and distribution of melanosomes, as well as their changes over time. This is helpful for understanding processes like melanin synthesis, transport and transfer in real-time.

To develop a compound screening strategy in the HTM system, we began with commonly used pigmentation-regulated compounds. As a substrate for melanin synthesis, L-Tyrosine is hydroxylated to form L-DOPA, which is further oxidized to dopaquinone, initiating melanin biosynthesis [9-11]. Increased L-tyrosine levels can enhance melanogenesis by stimulating tyrosinase activity and upregulating TYRP1 and TYRP2 expression in melanocytes [11-14]. Additionally, L-tyrosine promotes melanogenesis by enhancing melanosome biogenesis, maturation, and the trafficking of tyrosinase from the trans-Golgi network (TGN) to melanosomes [14-17]. Kojic Acid is a widely used skin-lightening agent that inhibits skin pigmentation through multiple mechanisms [18]. Its primary function in skin pigmentation is inhibiting melanin production through direct tyrosinase suppression [19-21]. By testing known pigmentation-related compounds using HTM, we can evaluate the reliability and accuracy of this image-based screening system.

2. Materials and Methods

Cell Culture

Human epidermal melanocytes, medium pigmented (HEMN_MP; Passage 3) were obtained. (CellnTec, Switzerland). Cells were pre-cultured in CnT-40 melanocyte culture medium (CellnTec) for one week. Then cells were seeded in 35 mm ibidi dishes (ibidi GmbH, Germany) with a glass coverslip bottom, at an initial confluency of 25%. This corresponded to approximately 5×10^4 cells per dish. The cells were incubated overnight at 37°C in a humidified atmosphere containing 5% CO_2. After overnight culture, the cells reached approximately 50% confluency 40-50% (~1×10^5 cells), at which point they were used for further testing.

Live-Cell Imaging by Holotomographic Microscopy

Live-cell imaging was performed using a Nanolive holotomographic microscope to assess morphological and dynamic changes in HEMN_MP cells following treatment with selected compounds. Prior to imaging, the culture medium was removed and replaced with 1 mL of fresh CnT-40 medium, either with or without test compounds.

Cells were divided into four treatment groups:

1) Non-treated control
2) Kojic Acid at a final concentration of 3.52 mM (0.05%)
3) L-Tyrosine at 500 µM (0.009%)
4) Combination of Kojic Acid and L-Tyrosine

After a 3-hour incubation period under standard culture conditions (37°C, 5% CO_2), the cells were immediately subjected to holotomographic imaging. Image acquisition was performed using a Nanolive 3D Cell Explorer microscope in 5 × 5 grid-scan mode, providing a total field of view of 394 × 394 µm. Time-lapse images were captured every 7 minutes and 30 seconds for all four groups simultaneously. The entire imaging session lasted approximately 5 hours, allowing for real-time monitoring of cellular responses to treatment.

Melanosome quantification

Melanosome quantification was performed using two complementary image analysis approaches: Nanolive's EVE software and ImageJ (NIH, USA), to evaluate melanosome distribution and abundance following compound treatment.

Images were analyzed using EVE Analyze, the AI-based analysis software provided by Nanolive. The Lipid Droplet Assay module was utilized to approximate melanosome-like organelles based on their refractive index characteristics. The key parameter used was "the

mean lipid droplet count per cell", with the segmentation sensitivity set at 0.9 to optimize detection of cytoplasmic vesicles. The "perimeter" was evaluated as an indicator of particle size. Quantified data were used to generate curves showing temporal changes across treatment groups.

To specifically quantify melanosomes per cell, image frames taken between 3 to 6 hours post-treatment were analyzed in ImageJ. For each treatment group, 7–9 individual cells exhibiting visible melanosomes were selected. Image preprocessing included setting a manual threshold to highlight melanosome-like dots within the cytoplasmic region, avoiding inclusion of nuclear structures. The "Analyze Particles" plug-in was then applied with a particle size range of 0.09 μm² – 1 μm² (corresponding to a diameter of approximately 0.3 μm – 1 μm), to count discrete melanosome-like particles per cell [22].

For melanosome distribution, image analysis was performed using FIJI (ImageJ) to quantify the spatial distribution of particles relative to the population centroid. First, particles were segmented using appropriate thresholding and particle analysis tools to extract their (X_i, Y_i) coordinates. The population centroid (X_0, Y_0) was calculated as the mean of all particle coordinates:

$$X_0 = \frac{1}{n}\sum_{i=1}^{n} X_i, \quad Y_0 = \frac{1}{n}\sum_{i=1}^{n} Y_i$$

The Euclidean distance (D_i) of each particle to the centroid was computed using the formula:

$$D_i = \sqrt{(X_i - X_0)^2 + (Y_i - Y_0)^2}$$

The mean distance ($\overline{D}$) from each particle to the population centroid was calculated.

Statistical analysis was performed by reporting the mean ± standard error of the mean (S.E.M.). All measurements were calibrated using a scale bar for pixel-to-micron conversion. A p-value of less than 0.05 was considered statistically significant.

3. Results

Distinguishing melanosomes using HTM and validation of melanosome content using EVE software with known pigmentation-regulating compounds.

We first assessed whether melanosomes could be detected using HTM and its internal analysis software, EVE. Human melanocytes were treated with either L-tyrosine or Kojic Acid at specified concentrations. The refractive index (RI)-based image displayed high-resolution details of the melanocytes, clearly revealing the cell structure and components. Particles with high RI are distinctly visible within the cells. The RI of melanosomes is higher than that of the surrounding cytoplasm in melanocytes, allowing clear visualization of these particles within the cells [8]. Although the RI of lipid droplets is slightly lower than that of melanosomes, it remains higher than that of the cytoplasm and can be distinguished using HTM [23]. While lipid droplets are ubiquitous in most cell types for energy storage, no studies in the provided results mention lipid droplets in melanocytes, suggesting they are either rare or not functionally relevant in these specialized cells under normal conditions. Therefore, we assume that most of the observed particles are melanosomes rather than lipid droplets. We observed that not all cells contained particles, likely due to the cells being at different stages of development (**Fig. 1A**).

Melanosome content was measured using AI-baed analysis software: EVE under the parameter "Mean Lipid Droplets Count Per Cell," which quantifies the number of particles per cell by dividing the total particle count by the number of cells in the area (**Fig. 1B**).

We determined that the optimal cell confluency for initiating compound treatment and imaging is 40-50%. At this confluency, cells form a single layer on the culture dish, ensuring

both uniform distribution and sufficient melanosome-containing cells for analysis. Time-lapse imaging was initially performed using HTM for up to 1 day. However, maintaining high image quality and accurate post-processing requires a single-cell layer. Due to cell proliferation, imaging quality declined, making further analysis unreliable. Therefore, in subsequent experiments, quantification data is measured between 3-8 hour time point.

L-Tyrosine is expected to increase melanin production and melanosome amount, while Kojic Acid reduces them [12, 15, 19, 20]. The results showed that L-tyrosine treatment led to a maximal 1.5-fold increase in melanosome number compared to the control. In contrast, Kojic Acid treatment significantly reduced melanosome counts to half that of the control during the time. Interestingly, when cells were treated with both tyrosine and Kojic Acid, melanosome content remained comparable to the control for the majority of the treatment period (**Fig. 1C**). These results are consistent with previously reported data, supporting the accuracy of the parameters used. They also suggest that the particles observed are predominantly melanosomes.

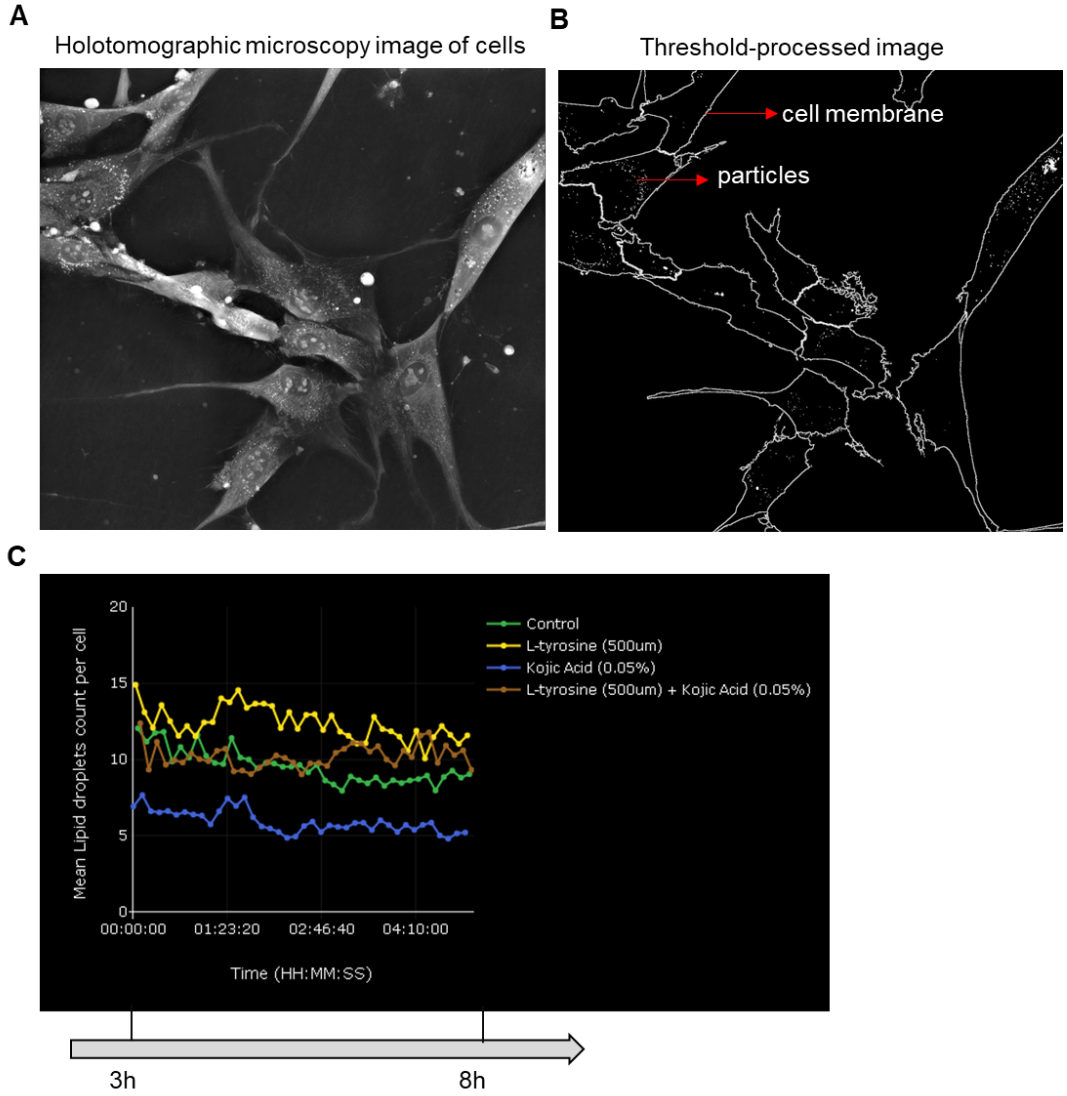

Figure 1. Quantification of melanosome quantity affected by L-Tyrosine and Kojic Acid using Nanolive EVE software. (A) Representative holotomographic image of a live cell acquired via Nanolive's 3D Cell Explorer. (B) Threshold-processed image of the same cell, highlighting melanosomes as particles. The delineated cell membrane facilitates accurate determination of cell boundar-

ies and number. (C) Graph shows the temporal dynamics of melanosome count per cell over a treatment period ranging from 3 to 8 hours. Data were analyzed using EVE Analytics.

Verification of melanosome content using FIJI

To further verify the reliability of the analysis performed by EVE, an alternative analysis was conducted using FIJI. We selected the 3–6-hour time frame, during which the compounds clearly took effect. As mentioned above, not all cells contain melanosomes, so we randomly selected 7-9 melanosome-containing cells from each group for analysis (**Fig. 2A**). As mentioned above, we applied a threshold with an RI higher than that of the nucleus, allowing us to directly measure the number of particles with a size (diameter^2) between 0.09–1 µm. The representative images for each group clearly show the presence of melanosomes within the cells (**Fig. 2A**). Compared to the control, L-tyrosine treatment resulted in both an increased number and noticeable accumulation of melanosomes. In contrast, Kojic Acid markedly reduced the number of particles. The combined treatment with both compounds resulted in an overall particle count similar to that of the control. Analysis using FIJI reveal differences in melanosome content among various active treatment groups (**Fig. 2B**). L-tyrosine increases melanosome levels to 2 times that of the control, while Kojic Acid reduces melanosome levels to 1/3 of the control. The combination maintains melanosome levels similar to the control. The FIJI analysis overall confirmed the results obtained by EVE. However, L-tyrosine treatment showed a higher fold increase when analyzed by FIJI compared to EVE. This is likely because EVE analysis is based on the total cell population, including cells that do not contain melanosomes. As a result, the melanosome count per cell may be "diluted," buffering the observed fold increase.

In conclusion, the HTM shows high quality of images and the parameter "Mean Lipid Droplets Count Per Cell" is a reliable measure for monitoring melanosome content over time and can be applied in further studies.

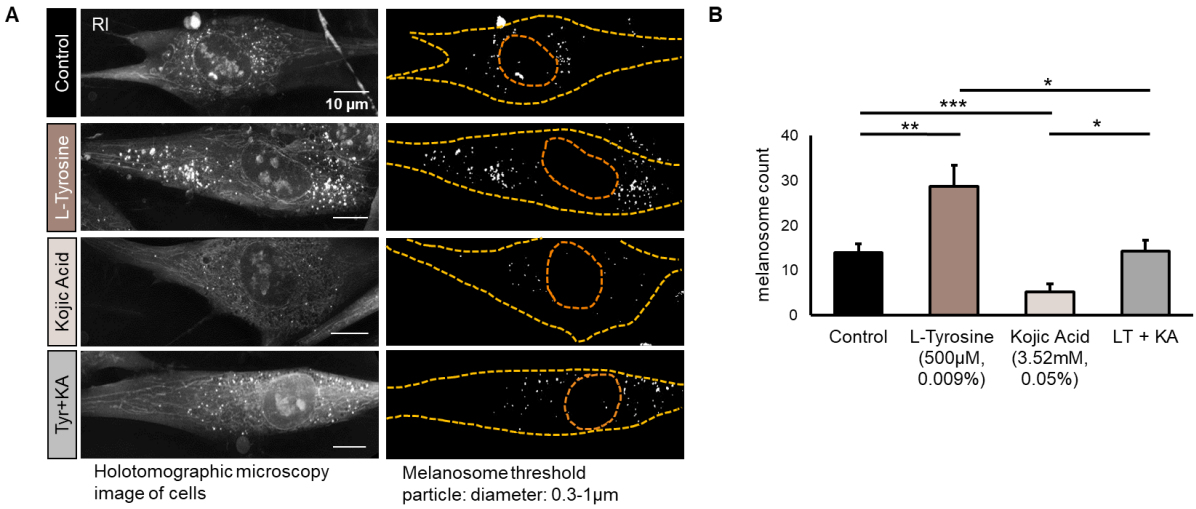

Figure 2. Quantification of melanosome quantity affected by L-Tyrosine and Kojic Acid using FIJI. (A) Representative holotomographic images of live cells from various treatment groups, acquired using Nanolive's 3D Cell Explorer. The left panel displays raw images highlighting cellular structures, while the right panel presents threshold-processed images where melanosomes are visualized as distinct particles. The delineation of the cell membrane and nucleus facilitates accurate identification of individual cells. (B) Quantitative analysis of melanosome content in 7–9 representative cells per treatment group, assessed at 3 to 8 hours post-treatment. Image analysis was performed using FIJI software, revealing significant differences in melanosome numbers among the various treat-

ment conditions. Data are presented as mean ± standard error of the mean (S.E.M). Statistical significance was determined using T-tests: $p < 0.05$ (*), $p < 0.01$ (**), $p < 0.005$ (***).

Verification of melanosome distribution using FIJI

We observed from the image that melanosomes are diffused from the perinuclear region, especially in the L-tyrosine treatment (**Fig. 3A**). Therefore, we designed a parameter using FIJI to calculate the mean distance of melanosomes to the centroid. The schematic for defining the coordinates of particles and the centroid is shown in **Fig. 3B**. The computing formula is described in the Materials and Methods section. The parameter of melanosome distribution, shown in **Fig. 3C**, indicates that L-tyrosine increases the mean distance of melanosomes to the centroid by 1.5 times compared to the control. Kojic Acid slightly reduces this distance; however, when combined with L-tyrosine, it appears unable to promote perinuclear melanosome localization, as the combination does not reduce the distance compared to L-tyrosine treatment alone.

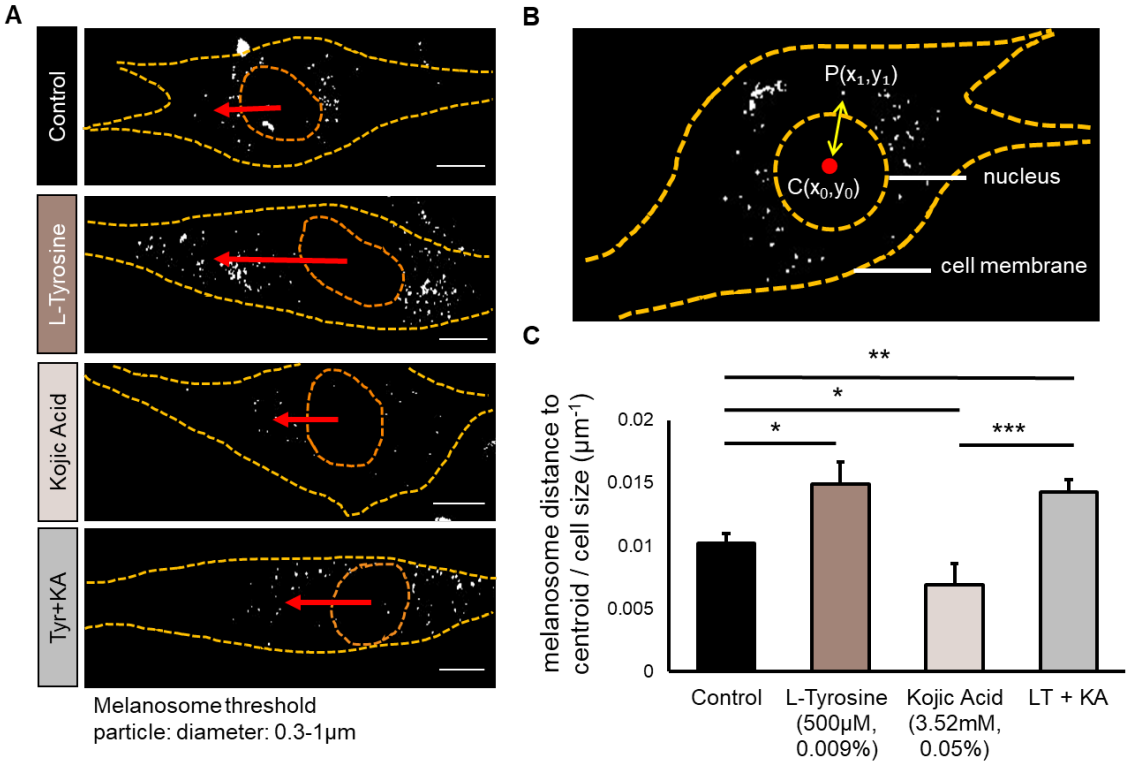

Figure 3. Quantification of melanosome distribution affected by L-Tyrosine and Kojic Acid using FIJI. (A) Threshold-processed images from Figure 2, highlighting melanosomes as distinct particles. Red arrows indicate the schematic measurement of the distance from each melanosome to the nucleus. (B) Schematic representation showing the coordinates of individual melanosomes and the centroid of the nucleus, facilitating precise distance measurements. (C) Quantitative analysis of mean melanosome distance/cell size in 7–9 representative cells per treatment group, assessed at 3 to 8 hours post-treatment. Image analysis was performed using FIJI software, revealing significant differences in melanosome distribution among the various treatment conditions. Data are presented as mean ± standard error of the mean (S.E.M). Statistical significance was determined using T-tests: $p < 0.05$ (*), $p < 0.01$ (**), $p < 0.005$ (***).

4. Discussion

Interpretation of the effects of known compounds on melanosome dynamics using HTM

The Nanolive HTM enabled real-time visualization of melanosome/pigment granule dynamics with high-resolution imaging. Subsequent analysis using various software tools provided precise quantitative data.

L-Tyrosine and Kojic Acid are known to both target tyrosinase in the melanogenesis pathway [13,14,19, 20]. The combination of L-tyrosine and Kojic Acid shows overall similar melanosome contents to the control, suggesting that Kojic Acid can counteract the tyrosine-induced stimulation of melanogenesis. However, the trend shown is not entirely stable (**Fig. 1C**). Since the observed trend reflects only the outcome of the interaction between these two compounds, the precise kinetics responses of human melanocytes to these compounds remain unclear. Nevertheless, this approach could be utilized in the future to screen compounds under conditions where cells are stimulated by factors such as a-MSH, UV exposure or oxidative stress [24, 25].

The observed distribution patterns of melanosomes are particularly intriguing, as they may relate to intracellular transport and transfer mechanisms. Although L-tyrosine is rarely reported to stimulate melanosome transfer, its treatment resulted in a more diffuse distribution of melanosomes. This effect may stem from a sudden surge in melanosome production, necessitating greater intracellular space and indirectly promoting the migration of melanin granules toward dendrites. This also applies to Kojic Acid. Kojic Acid itself has slightly promoted the perinuclear distribution of melanosomes, which may suggest a role in melanin transfer or intracellular migration. Overall, studying melanosome distribution offers a novel perspective on pigmentation parameters.

Future perspectives

While our system enables clearer and more specific visualization of each step in the pigmentation process, it primarily reveals observable phenomena rather than providing detailed mechanistic insights. To address this, additional assays are necessary, such as testing the effects of compounds on specific biomarkers directly [4].

Nevertheless, the system offers a quick and cost-effective screening strategy, providing researchers with a preliminary overview of a compound’s effects on pigmentation and laying the foundation for more in-depth research.

Mimicking the complex physiological environment of human skin in vitro remains a challenge. A promising approach to studying cell interactions and material exchange is through co-culture systems that incorporate multiple cell types. For instance, combining holotomography microscopy with a melanocyte-keratinocyte co-culture could enable direct visualization of melanin transfer between cells.

In conclusion, our novel assay, which visualizes melanosome movement in live cells using holotomography microscopy, offers an innovative approach to studying skin pigmentation. Future advancements will involve integrating both image-based and molecular-based assays, allowing for a more comprehensive evaluation of pigmentation-related products and treatments.

5. Conclusion

In conclusion, this study demonstrates that holotomographic microscopy (HTM) is a powerful, label-free imaging technique for real-time visualization of melanosome dynamics in living cells. By capturing high-resolution images, HTM enables detailed analysis of melanosome amount, distribution and movement, providing valuable insights into the effects of compounds like L-Tyrosine and Kojic Acid on melanogenesis and melanin migration. This

approach offers a novel perspective for cosmetic research, facilitating the development of targeted skincare products aimed at controlling pigmentation.

6. Reference

1. D'Mello, S.A., et al., *Signaling Pathways in Melanogenesis.* Int J Mol Sci, 2016. **17** (7).
2. Raposo, G. and M.S. Marks, *Melanosomes--dark organelles enlighten endosomal membrane transport.* Nat Rev Mol Cell Biol, 2007. **8**(10): p. 786-97.
3. Bento-Lopes L, C.L., Charneca J, Neto MV, Seabra MC, Barral DC. , *Melanin's Journey from Melanocytes to Keratinocytes Uncovering the Molecular Mechanisms of Melanin Transfer and Processing.* Int J Mol Sci., 2023.
4. Singh, P., et al., *Cell-Based Model Systems for Validation of Various Efficacy-Based Claims for Cosmetic Ingredients.* Cosmetics, 2022. **9**(5): p. 107.
5. Sandoz, P.A., et al., *Image-based analysis of living mammalian cells using label-free 3D refractive index maps reveals new organelle dynamics and dry mass flux.* PLoS Biol, 2019. **17**(12): p. e3000553.
6. Medina-Ramirez, I.E., et al., *Holotomography and atomic force microscopy: a powerful combination to enhance cancer, microbiology and nanotoxicology research.* Discov Nano, 2024. **19**(1): p. 64.
7. Liu, P.Y., et al., *Cell refractive index for cell biology and disease diagnosis: past, present and future.* Lab Chip, 2016. **16**(4): p. 634-44.
8. Song, W., et al., *Wavelength-dependent optical properties of melanosomes in retinal pigmented epithelium and their changes with melanin bleaching: a numerical study.* Biomed Opt Express, 2017. **8**(9): p. 3966-3980.
9. Olivares, C., J.C. Garcia-Borron, and F. Solano, *Identification of active site residues involved in metal cofactor binding and stereospecific substrate recognition in Mammalian tyrosinase. Implications to the catalytic cycle.* Biochemistry, 2002. **41** (2): p. 679-86.
10. Snyman, M., et al., *The metabolism of melanin synthesis-From melanocytes to melanoma.* Pigment Cell Melanoma Res, 2024. **37**(4): p. 438-452.
11. Slominski, A., et al., *Positive regulation of melanin pigmentation by two key substrates of the melanogenic pathway, L-tyrosine and L-dopa.* J Cell Sci, 1988. **89 (Pt 3)**: p. 287-96.
12. Hirobe, T., et al., *Excess tyrosine rescues the reduced activity of proliferation and differentiation of cultured recessive yellow melanocytes derived from neonatal mouse epidermis.* Eur J Cell Biol, 2007. **86**(6): p. 315-30.
13. Slominski, A. and R. Costantino, *L-tyrosine induces tyrosinase expression via a posttranscriptional mechanism.* Experientia, 1991. **47**(7): p. 721-4.
14. Slominski, A., et al., *Melanin pigmentation in mammalian skin and its hormonal regulation.* Physiol Rev, 2004. **84**(4): p. 1155-228.
15. Hirobe, T., et al., *Stimulation of the proliferation and differentiation of mouse pink-eyed dilution epidermal melanocytes by excess tyrosine in serum-free primary culture.* J Cell Physiol, 2002. **191**(2): p. 162-72.

16. Rosemblat, S., et al., *Melanosomal defects in melanocytes from mice lacking expression of the pink-eyed dilution gene: correction by culture in the presence of excess tyrosine.* Exp Cell Res, 1998. **239**(2): p. 344-52.
17. Slominski, A., G. Moellmann, and E. Kuklinska, *L-tyrosine, L-dopa, and tyrosinase as positive regulators of the subcellular apparatus of melanogenesis in Bomirski Ab amelanotic melanoma cells.* Pigment Cell Res, 1989. **2**(2): p. 109-16.
18. Saeedi, M., M. Eslamifar, and K. Khezri, *Kojic acid applications in cosmetic and pharmaceutical preparations.* Biomed Pharmacother, 2019. **110**: p. 582-593.
19. Cabanes, J., S. Chazarra, and F. Garcia-Carmona, *Kojic acid, a cosmetic skin whitening agent, is a slow-binding inhibitor of catecholase activity of tyrosinase.* J Pharm Pharmacol, 1994. **46**(12): p. 982-5.
20. Wang, W., et al., *Kojic Acid Showed Consistent Inhibitory Activity on Tyrosinase from Mushroom and in Cultured B16F10 Cells Compared with Arbutins.* Antioxidants (Basel), 2022. **11**(3).
21. Saghaie, L., et al., *Synthesis and tyrosinase inhibitory properties of some novel derivatives of kojic acid.* Res Pharm Sci, 2013. **8**(4): p. 233-42.
22. Okada, T., et al., *Structural analysis of melanosomes in living mammalian cells using scanning electron-assisted dielectric microscopy with deep neural network.* Comput Struct Biotechnol J, 2023. **21**: p. 506-518.
23. Chen, X., et al., *Lipid droplets as endogenous intracellular microlenses.* Light Sci Appl, 2021. **10**(1): p. 242.
24. Nguyen, N.T. and D.E. Fisher, *MITF and UV responses in skin: From pigmentation to addiction.* Pigment Cell Melanoma Res, 2019. **32**(2): p. 224-236.
25. Kim, N.H. and A.Y. Lee, *Oxidative Stress Induces Skin Pigmentation in Melasma by Inhibiting Hedgehog Signaling.* Antioxidants (Basel), 2023. **12**(11).